Title
Spin-density wave in polycrystalline Cr films from infrared reflectivity

Journal
Physical Review B, 76(22)

ISSN
2469-9950

Authors
Boekelheide, Z
Helgren, E
Hellman, F

Publication Date
2007-12-01

DOI
10.1103/physrevb.76.224429

Peer reviewed

Spin-density wave in polycrystalline Cr films from infrared reflectivity

Z. Boekelheide,* E. Helgren, and F. Hellman
Department of Physics, University of California, Berkeley, Berkeley, California 94720, USA
(Received 15 September 2007; published 26 December 2007)

The spin-density wave properties of polycrystalline chromium thin films were determined by using infrared reflectivity to determine the gap energies. The incommensurate spin-density wave of bulk chromium is highly sensitive to perturbations from stress, disorder, and finite size effects, such as those found in polycrystalline films. Films prepared under various conditions display three different types of spin-density wave behavior: incommensurate, commensurate, and mixed. Unexpectedly, the mixed phase includes the incommensurate spin-density wave and two different forms of commensurate spin-density wave. A phenomenologically determined low-temperature phase diagram is created to describe the spin-density wave in chromium in the stress-disorder plane. The effects of stress and disorder on the spin-density wave of chromium films are analogous to the effects of dilute alloying in bulk chromium. In this case, tensile stress has a similar effect to Mn impurities, while disorder has a similar effect to Al.

DOI: 10.1103/PhysRevB.76.224429 PACS number(s): 75.30.Fv, 75.70.−i, 78.30.−j, 68.55.−a

I. INTRODUCTION

Chromium, as a spin-density-wave (SDW) material, has unique and extremely complex properties and has been the focus of significant research. Prior to 1988, most research on Cr focused on bulk samples and produced intricate phase diagrams in experiments that varied temperature, pressure, and binary and ternary alloying. The 1988 discovery of giant magnetoresistance (GMR) in Fe/Cr multilayers inspired further research on the SDW in Cr and shifted the focus of that research toward films and multilayers, where other variables such as thickness, strain, and disorder are crucial.

The SDW in bulk Cr is incommensurate (ISDW), meaning that the wavelength is not an integer number of lattice constants. The transition to the paramagnetic state occurs at a Néel temperature (T_N) of 311 K. Small perturbations to the structure change the SDW to commensurate (CSDW), where the wavelength is an integer number of lattice constants, or to the paramagnetic state. The classic example of this sensitivity is that adding 0.3–1.0 at. % Mn into bulk Cr introduces a CSDW phase between the low-temperature ISDW and high-temperature paramagnetic phases; above 1.0 at. % Mn, the ISDW phase is entirely replaced by the CSDW. On the other hand, with the addition of V, the ISDW remains, but the Néel temperature slowly decreases until 4 at. % V, at which point the resulting material is paramagnetic at all temperatures. The explanation given for this is that the electron concentration is increased with the addition of Mn, while it is decreased with the addition of V (Cr has six valence electrons per atom, Mn has seven, and V has five). The change in electron concentration disrupts the delicate Fermi surface nesting responsible for the ISDW.[1]

In experiments involving thin films, the effects of physical confinement have been a main focus. Recent angle resolved photoemission spectroscopy (ARPES) measurements on epitaxial Cr(110) give direct evidence of band structure changing with film thickness in the range 30–120 Å.[2] In this thickness range, the low-temperature state is ISDW, with a phase transition to CSDW at higher temperatures. In addition, studies on exchange-biased epitaxial Fe/Cr(001) layers show that the ISDW wave vector differs from bulk at thicknesses as large as 1100 Å.[3] Below 1100 Å, T_N decreases from the bulk value of 311 K, and the period of the ISDW increases.

While excellent work has been done on epitaxial films, and indeed measurements such as ARPES require epitaxy, many of the Fe/Cr multilayers studied in the literature are polycrystalline. In fact, the degree of disorder in a multilayer is an important variable, as some research has analyzed the effects of surface roughness on GMR.[4] The goal of this project was to understand the SDW in polycrystalline Cr films such as those commonly used in GMR multilayers, where disorder and stress are the important variables.

We expect that stress and disorder will have a strong impact on the SDW character of our films. Stress has been shown empirically to affect the SDW behavior of chromium in a similar way as the addition of Mn or V (Ref. 1). For example, hydrostatic pressure decreases the Néel temperature (like the addition of V), while tensile stress introduces a CSDW (like the addition of Mn). Neutron diffraction experiments done on crushed chromium powder samples (having both stress and disorder) have shown a CSDW phase present above the ISDW phase in temperature (a similar effect as adding about 0.5 at. % Mn), thought to be due to local strains. In addition, the transition between ISDW and CSDW was blurred, with the two phases coexisting between about 200 and 300 K.[5,6]

In bulk Cr, the ISDW is caused by nesting of the Fermi surface. A conceptual picture of the electron bands at the nesting site is given in Fig. 1(a). In the ISDW, there are two gaps, a direct gap with energy of 1000 cm^{-1} and an indirect gap with energy of 3600 cm^{-1} (Ref. 1), labeled here as Δ_1 and Δ_2.

The CSDW occurs when the two empty bands shown in Fig. 1(a) combine into one band instead of nesting next to each other [see Fig. 1(b)], for example, as a result of increasing the electron concentration. In that case, there is one direct gap, Δ_C. The energy of the commensurate gap has been calculated theoretically by Falicov and Penn[7] to be 2000 cm^{-1}, twice the energy of the incommensurate direct gap, and by Asano and Yamashita[8] to be 3200 cm^{-1}. Experimentally, the typical CSDW Cr dilute alloys Cr-Mn and Cr-Re are seen to

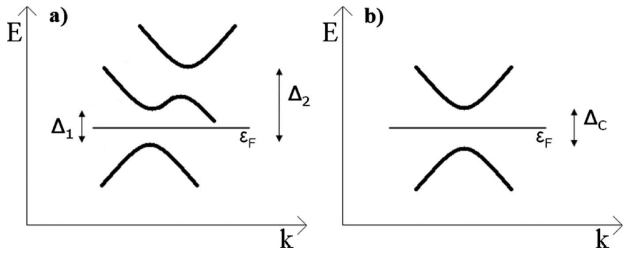

FIG. 1. (a) Conceptual model of bands in the ISDW state; Δ_1 is the direct gap and Δ_2 is the indirect gap. (b) Bands in the CSDW state with gap Δ_C.

have an energy gap between 2900 and 3200 cm^{-1} in the CSDW state.[1,9]

Another alloy, Cr-Al, with greater than 3 at. % Al, also has a CSDW structure based on neutron scattering,[10] but a gap of only 2400 cm^{-1} (Ref. 11) rather than the higher energies seen in Cr-Mn or Cr-Re alloys. Mn and Re, both group 7 transition metals, increase electron concentration when alloyed in Cr, causing the CSDW. In the case of Al, a nontransition metal, it is not clear how many electrons each Al atom contributes. Because of this, Cr-Al is not considered to be a typical CSDW alloy like Cr-Mn or Cr-Re. Experimentally, Cr-Al alloys have a high Néel temperature and high resistivity, which are not seen in other Cr alloys.[1] Cr-Al alloys with between 16 and 28 at. % Al show a nonmetallic behavior, with a negative temperature coefficient of resistance. Korringa-Kohn-Rostocker coherent-potential approximation band calculations have shown that Al atoms in substitutional sites behave very similar to vacancies in pure Cr because they do not participate in *d-d* bonding.[12] This causes significant scattering and can help explain the very high resistivities in Cr-Al alloys.

Infrared reflectivity as a function of frequency and temperature provides an excellent probe of the various SDW states of Cr. In this paper, we describe the results of reflectivity measurements on polycrystalline films prepared under various deposition conditions. We observed four distinct gaps: 1000, 2400, 3200, and 3600 cm^{-1}, which we compare to the gaps seen in bulk Cr and its alloys. Based on the energy gaps observed, we categorize each sample by its SDW behavior. We observe three basic types of SDW behavior: ISDW, CSDW, and mixed phase. We then explain the results in terms of the stress and amount of disorder present in each film.

II. EXPERIMENT

We sputtered 200 nm thick chromium films using an AJA magnetron sputtering system with a base pressure below 5×10^{-8} Torr. We varied the sputtering pressure between 0.75 and 8 mTorr. The gun was powered with 150 W dc, and the films were deposited at rates of 0.5–1.0 Å/s onto substrates of amorphous SiN_x-coated Si held at room temperature. In addition to this series, one sample was sputtered at 0.75 mTorr at 350 °C; this sample had larger grains and exhibited a bulklike behavior; in the rest of the paper, this will be referred to as the "bulklike" sample. One 150 nm sample was also grown by e-beam deposition at a very low base pressure ($<10^{-10}$ Torr), with the substrate held at room temperature. The samples, deposition conditions, and structural characteristics are summarized in Table I.

Scanning electron microscopy (SEM) and cross-sectional transmission electron microscopy (TEM) imaging showed columnar morphology. SEM shows top-down views of the columnar structure [Figs. 2(a)–2(c)], allowing us to calculate the lateral grain size. The film grown at 8 mTorr had the largest grains; these are oblong and 25×50 nm^2. The film grown at 0.75 mTorr had slightly smaller grains and more variation in grain size. The average grain is also oblong and 25×35 nm^2. The e-beam deposited sample showed very different structures from the sputtered samples, with some small round grains, some oblong grains, and some unusual multipronged grains. The average grain size for the e-beam sample was 15×50 nm^2. The bulk-like sputtered film was imaged with SEM, and no surface structure was visible, consistent with a very flat surface.

TEM images [see Figs. 2(d) and 2(e)] showed that the film grown at high argon pressure had a rough, jagged surface, while the film grown at low pressure was very flat. In addition, the films grown at high pressure had small grains at the base of the film (7 nm) growing into larger grains in the bulk with an average size of 18 nm, with small amounts of

TABLE I. Table of samples used in this study: their growth properties, grain size, stress, residual resistivity, and Néel temperatures. Sputtered samples were 200 nm thick, and the e-beam sample was 150 nm.

Sample	Growth technique	Substrate temperature	Sputter pressure (mTorr)	Grain size from XRD (nm)	Tensile stress (MPa) (±10%)	Residual resistivity ($\mu\Omega$ cm)	Néel temperature (K)
e-beam	e-beam	RT	N/A	19	900 (±30%)	20	250
Bulklike	Sputter	350 °C	0.75	35	580	6	300
0.75 mTorr	Sputter	RT	0.75	22	1310	16	>400
1.3 mTorr	Sputter	RT	1.3	19	1650	23	>400
2 mTorr	Sputter	RT	2	18	1290	32	>400
4 mTorr	Sputter	RT	4	22	580	100	262
6 mTorr	Sputter	RT	6	25	480	194	270
8 mTorr	Sputter	RT	8	28	260	402	221

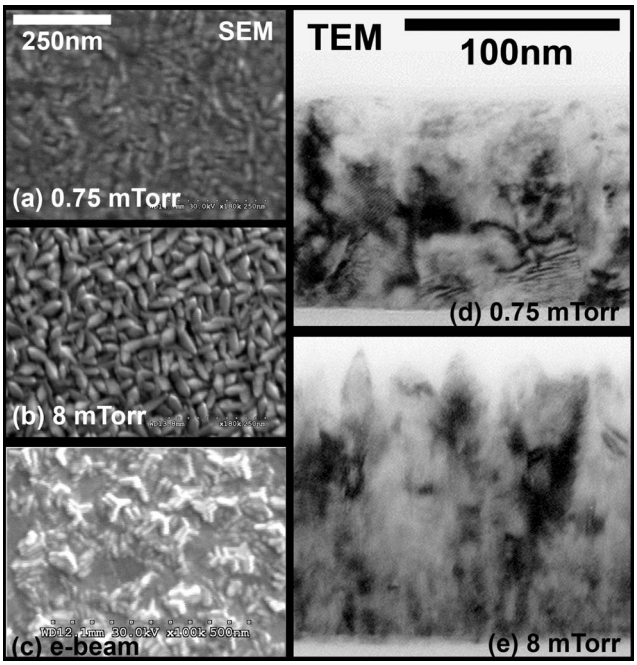

FIG. 2. [(a)–(c)] SEM top-down images of samples: (a) 0.75 mTorr, (b) 8 mTorr, and (c) e-beam. The bulklike film was also imaged by SEM, and no structure was observed. [(d) and (e)] Cross-sectional TEM images: (d) 0.75 mTorr (100 nm), (e) 8 mTorr (130 nm). TEM was done on 100 and 130 nm thick films.

amorphous material observed between columns. Because of the difference between materials at or near the column boundaries (including some amorphous materials) and materials far from the column boundaries, as well as the grain growth with thickness, we consider these films to be inhomogeneous. The films grown at low pressure had a less well-defined columnar morphology, with no amorphous material observed and approximately 29 nm grains throughout; we consider these films to be homogeneous. The TEM images shown are of 100 and 130 nm thick films, while the SEM and other experiments were done on 200 nm thick films; the smaller lateral grain size observed in the TEM compared to the SEM images of the 8 mTorr sample is due to the grain growth with thickness in this sample.

X-ray diffraction was used to verify the Cr bcc structure and showed no exotic crystal phases. While SEM gives the grain size in the lateral direction, the x-ray peak width allowed us to calculate the out-of-plane grain size. Grain size was determined from the dominant (110) peak width and was not strongly dependent on sputtering pressure.[13] These grain sizes are significantly smaller than the thickness; although the grain growth is columnar, defects break the coherence and lead to the grain sizes shown in Table I.

Energy dispersive x-ray spectroscopy (EDS) done at 10 keV showed no Ar, N, or C contamination of the films, within the margin of error of 0.25 at. % for Ar and N, and 1.0 at. % for C (Ref. 14). The total oxygen percentage was 2 at. % in the films grown at low pressure and the e-beam sample, and 4 at. % in the films grown at high pressure. Chromium is known to form a self-limiting oxide, and these EDS results are consistent with a surface oxide layer, given that the films grown at high pressure were rough and had about twice the surface area to oxidize. A simple calculation shows that if the measured 2 at. % oxygen is located entirely at the surface in the form of Cr_2O_3, that surface oxide would consume the top 3 nm of Cr, leading to a 6 nm oxide layer. This is reasonable for a self-limiting oxide layer. There was no difference in O at. % between films kept in air and those kept in a vacuum dessicator.

Stress was measured using a Tencor FLX-2320 stress measurement system. The Tencor measures the curvature of a 4 in. Si wafer before and after a film is deposited. The stress in MPa is calculated from the difference in the two wafer curvature profiles using the material properties of the Si substrate and the thickness of the film deposited. For the e-beam deposited sample, it was not possible to deposit onto a 4 in. wafer, so the stress was obtained indirectly from x-ray peak position measurements.[15] The stress of each film is noted in Table I. Stress in sputtered films can be either compressive or tensile depending on the atomic weights of the sputtered material and sputtering gas, as well as the sputtering pressure and source-substrate distance;[16,17] here, we are in the tensile regime for all pressures. E-beam deposition also typically results in tensile stress (in the absence of epitaxy or differential thermal contraction).[18]

Electrical resistivity (ρ) vs temperature was measured by a four point method. We do not show the temperature profiles here; however, the low-temperature resistivity is strongly dependent on growth parameters, especially sputtering pressure, ranging from 5 to 400 $\mu\Omega$ cm, consistent with literature.[19] The residual resistivity (ρ_0) values are tabulated in Table I.[20] The Néel temperature can be seen in $\rho(T)$; we locate the Néel temperature by the minimum in $d\rho/dT$.[21] For our samples, the resistivity anomaly was quite broad due to the effects of strain and polycrystallinity. Three samples (0.75, 1.3, and 2 mTorr) had Néel temperatures higher than what we were able to measure (400 K).

Infrared reflectivity was measured using a Bruker Fourier transform infrared (FTIR) model 66v-S at beamline 1.4 of the Advanced Light Source. Each sample, along with a gold mirror, was mounted inside a cryostat with a KBr optical window, which was then placed into the FTIR. The cryostat and the FTIR optics were under a rough vacuum. For each measurement, the reflectivity spectrum was measured 64 times and averaged using the OPUS software; the same was done for the gold mirror to measure the background. Finally, the sample spectrum was divided by the background to give the reflectivity spectrum from the sample. Reflectivity was measured for each sample at multiple temperatures.

III. RESULTS

The mid-IR reflectivity for each sample was measured as a function of temperature in order to observe the SDW gap features in the spectrum expected to occur in the range between 800–4000 cm^{-1}. We took data in the range 500–7000 cm^{-1} and applied an adjacent-averaging smoothing technique with a width of 100 cm^{-1} over most of the data set. Above 4500 cm^{-1}, the intensity of the mid-IR lamp was lower, leading to a higher noise level, so in this region we

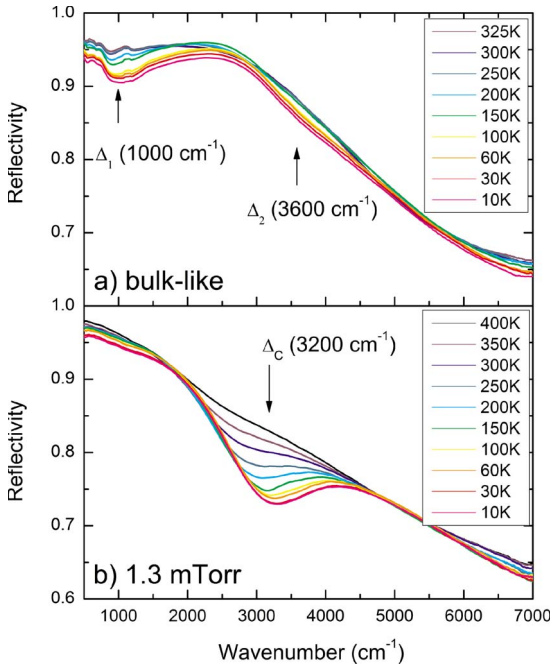

FIG. 3. (Color online) Reflectivity of (a) bulklike and (b) 1.3 mTorr samples at temperatures between 10 and 400 K.

used a smoothing width of 300 cm^{-1}. Example data sets are shown for the bulklike sample in Fig. 3(a) and the 1.3 mTorr sample in Fig. 3(b). In Fig. 3, we see that the reflectivity of both samples generally decreases with wave number for all temperatures. In addition, at low-temperature gaps are observed, which disappear as the temperature is increased.

In order to clearly determine the SDW energy gaps and to compare them to literature, we focus primarily on the low-temperature (10 K) reflectivity and the reflectivity ratio (RR), which is the ratio of the low-temperature reflectivity to that at high temperature (above the Néel temperature). To plot the RR, we have determined a Néel temperature for each film from a minimum in $d\rho/dT$, shown in Table I. For the low pressure samples, the Néel temperature could not be reached in the reflectivity apparatus, so data at the maximum temperature (400 K) were used as an approximation. Figure 3(b) shows that in the 1.3 mTorr sample the SDW gap at 3200 cm^{-1} is nearly gone by 400 K; similar data were found for the 0.75 and 2 mTorr samples (not shown). Thus, the Néel temperature is not significantly higher than 400 K, so using the 400 K data for the reflectivity ratio is a good approximation.

The reflectivity at 10 K is plotted for all samples in Figs. 4(a)–4(c) and the RR in Figs. 4(d)–4(f). The data show three distinct SDW behaviors at low temperature. Two exhibit the ISDW seen in bulk Cr (the bulklike and e-beam samples), three exhibit a CSDW, as seen in Cr-Mn (the sputtered samples grown at the lowest pressures), and three show gaps corresponding to multiple SDW phases (the sputtered samples grown at the highest pressures). The data in Fig. 4 are separated into these three distinct SDW behaviors.

The reflectivities of the ISDW samples are shown in Fig. 4(a), with the reflectivity of bulk Cr plotted for comparison. The reflectivities of both films closely resemble that of bulk, with the gap at Δ_1 apparent; the indirect gap at Δ_2 is not obvious in either sample or in bulk Cr. The reflectivity of the commensurate SDW samples is shown in Fig. 4(b), with the reflectivity of two typical CSDW alloys, Cr-Mn and Cr-Re, plotted for comparison. We see the commensurate gap Δ_C at a wave number of 3200 cm^{-1}, within the range of observed commensurate gap energies seen in Cr-Mn and Cr-Re. The three samples with mixed SDW are shown in Fig. 4(c), with bulk Cr plotted for comparison. The reflectivities of these three films are quite different from the bulk, with a lower absolute reflectivity overall and no features readily apparent.

We now turn to the reflectivity ratio, plotted for the ISDW samples in Fig. 4(d), for the CSDW samples in Fig. 4(e) and for the mixed SDW samples in Fig. 4(f). For the ISDW samples, plotting the ratio reveals the broad gap at Δ_2 that was difficult to notice in the absolute reflectivity. For the CSDW samples, an interesting result of plotting the ratio is that while the dip in the reflectivity looks somewhat different for the three samples, the gap energy Δ_C (3200 cm^{-1}), as seen in the ratio, is actually extremely close for all three film samples. Also, the 2 mTorr sputtered sample shows a small but visible dip, a Δ_1, which suggests that the sample has small regions of ISDW, although we still classify this film as CSDW. In what we have called the mixed SDW samples, three features are evident. First, the ISDW direct gap Δ_1 is visible, although broadened somewhat perhaps due to disorder. The indirect gap Δ_2 is not clear; possibly it is broadened so much that we cannot see it at all. In addition, there is a small dip at Δ_C, showing that parts of the films have CSDW. Finally, we observe an additional gap at 2400 cm^{-1}, labeled as Δ_X. We recognize this gap energy as the same one seen in the atypical CSDW Cr-Al alloys,[11] also plotted in Fig. 4(e) for reference. We conclude that the Cr samples grown at 4, 6, and 8 mTorr have multiple coexisting phases: ISDW (as in bulk Cr) and two distinct forms of CSDW (as in Cr-Mn and Cr-Al). Because we know that these films are morphologically inhomogeneous, as evidenced from the TEM image of the 8 mTorr film, it is not surprising that ISDW and CSDW coexist; however, the fact that we see two distinct CSDW gaps is surprising.

Previous research on Cr and its dilute alloys has often shown CSDW occurring as a high-temperature phase, with ISDW as a low-temperature phase (rarely the other way around).[1] In order to determine the temperature dependence of the SDW in our films, we plot the reflectivity ratios for a range of temperatures to see how the gaps change with temperature. These data are plotted for a representative sample of each type in Fig. 5. Figure 5(a) shows the bulklike sample; the closing of the two ISDW gaps is visible up to 300 K, consistent with our measured Néel temperature of 300 K. In Fig. 5(b), we show the 1.3 mTorr sample; again the CSDW gap (Δ_C) is seen closing up to 375 K, consistent with a Néel temperature slightly above 400 K. The 4 mTorr sample is shown in Fig. 5(c). We see that the gap at 1000 cm^{-1} (Δ_1) and the one at 3200 cm^{-1} (Δ_C) disappear by 200 K. In addition, the second ISDW gap (Δ_2), which could not be distinguished previously, is now visible as a slight depression at 3600 cm^{-1}, which also disappears by 200 K. The Néel tem-

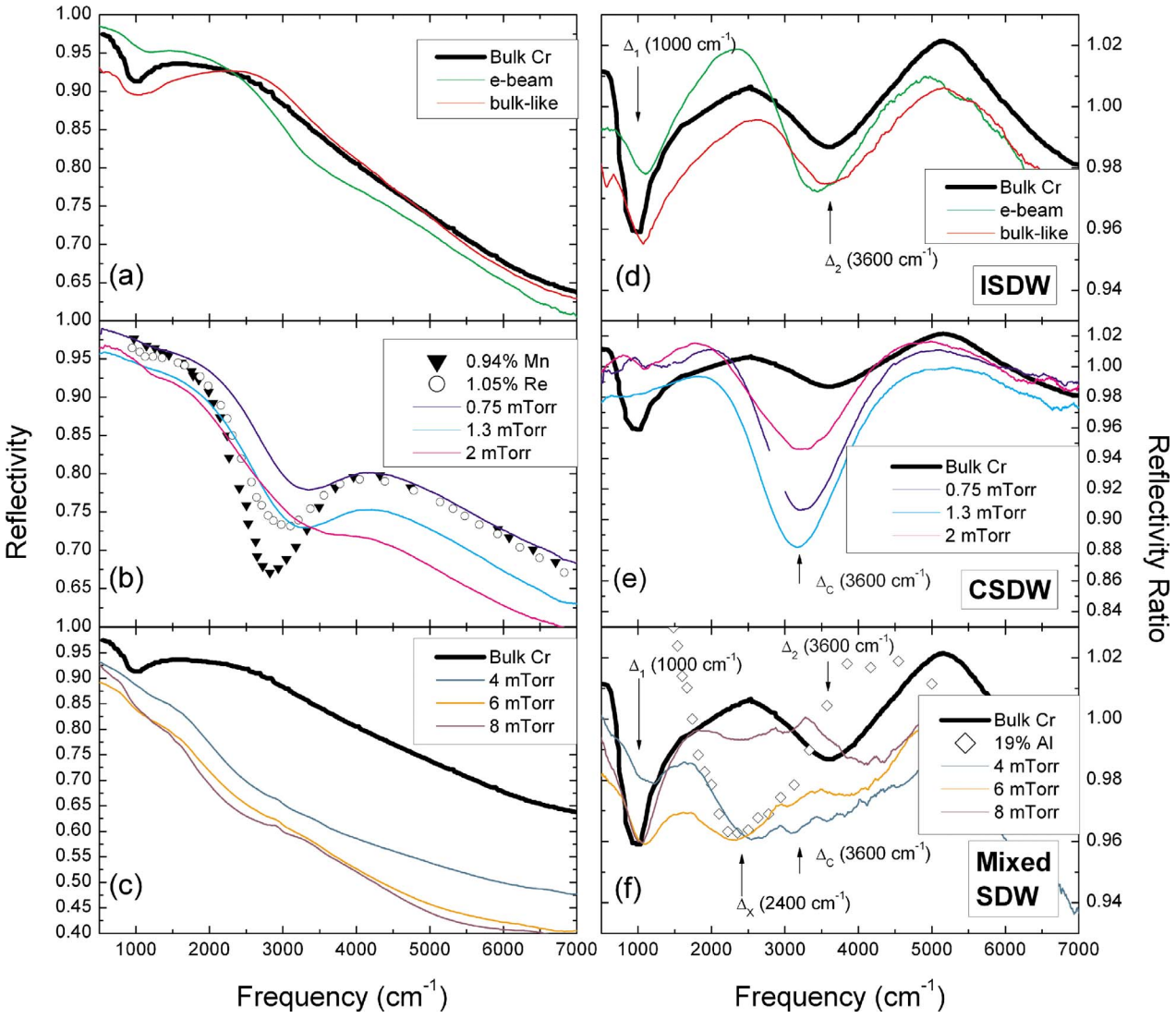

FIG. 4. (Color online) Reflectivity at 10 K of (a) ISDW samples (bulklike and e-beam) compared to bulk Cr, (b) CSDW samples (0.75, 1.3, and 2 mTorr) compared to Cr-Mn and Cr-Re, and (c) mixed SDW samples (4, 6, and 8 mTorr) compared to bulk Cr. Reflectivity ratio ($R_{low\ temperature}/R_{paramagnetic}$) of (d) ISDW samples—bulklike ($R_{10\ K}/R_{325\ K}$) and e-beam ($R_{10\ K}/R_{400\ K}$) compared to bulk Cr, (e) CSDW samples—0.75, 1.3, and 2 mTorr ($R_{10\ K}/R_{400\ K}$), compared to bulk Cr (no Cr-Mn or Cr-Re RR data were available for comparison), and (f) mixed SDW samples—4, 6, and 8 mTorr ($R_{10\ K}/R_{400\ K}$, $R_{10\ K}/R_{350\ K}$, and $R_{10\ K}/R_{300\ K}$, respectively) compared to bulk Cr and Cr-Al. Bulk Cr reflectivity given at 30 K, ratio $R_{30\ K}/R_{325\ K}$ from Lind and Stanford (Ref. 22), reflectivity at 4 K of Cr-Mn and Cr-Re alloys from Bos and Lynch (Ref. 9) and reflectivity ratio ($R_{30\ K}/R_{400\ K}$) of the Cr-Al alloy from Lind and Stanford (Ref. 11).

perature for this sample is 262 K, as measured by a minimum in $d\rho/dT$. Given the broad nature of the resistivity anomaly in these films, these temperatures are fairly consistent. Interestingly, the gap at 2400 cm^{-1} is still present up to at least 350 K. Thus, the measured resistivity anomaly in these films pertains only to the closing of the ISDW and one of the CSDW gaps (3200 cm^{-1}), while the other CSDW gap (2400 cm^{-1}) remains at higher temperatures. This point extends the comparison to Cr-Al alloys, which typically have high Néel temperatures.[1] The other CSDW (0.75, 2 mTorr) and mixed SDW (6, 8 mTorr) samples' behavior do not differ significantly from the representative data sets shown in Figs. 5(b) and 5(c).

The e-beam sample, which appeared from reflectivity and RR data to be ISDW and similar to the bulklike sample [see Figs. 4(a) and 4(d)], has a temperature dependent behavior that differs from the simple ISDW shown by the bulklike sample in Fig. 5(a). We show that behavior in Fig. 6. Figure 6(a) shows the reflectivity spectra at multiple temperatures. The two ISDW gaps Δ_1 and Δ_2 disappear by 200 K and, instead, a single gap opens, which looks similar to the CSDW gap observed in reflectivity in Fig. 4(b). This gap disappears again by 400 K. Figure 6(b) gives the reflectivity ratio, which shows clearly the transition from ISDW to CSDW at around 200 K. This is the only sample that shows such a transition. We refrain from stating the gap energy of this commensurate phase because quoted values for gap energy generally refer to the gap at zero temperature. The actual gap energy decreases with increasing temperature.

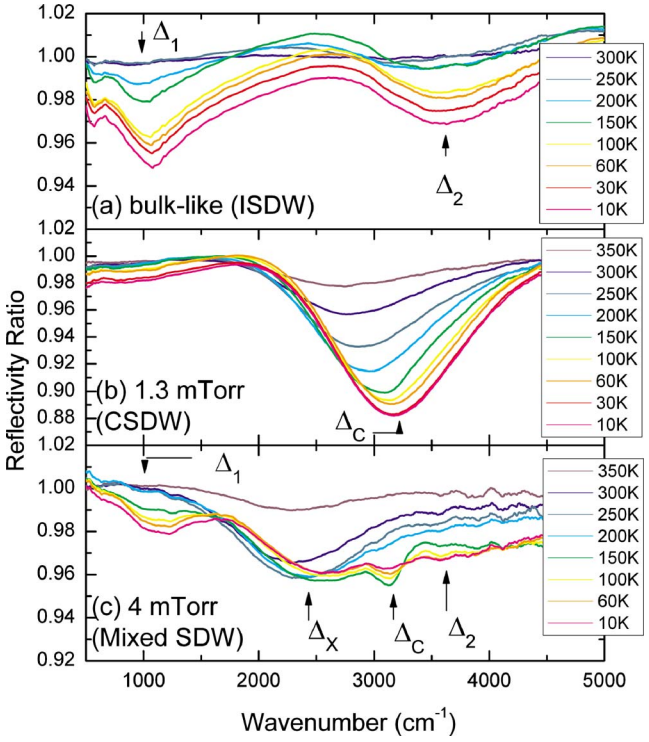

FIG. 5. (Color online) Reflectivity ratio (R_L/R_P) for R_L taken at multiple temperatures: (a) Bulklike sample (ISDW), (b) 1.3 mTorr sample (CSDW), and (c) 4 mTorr sample (mixed SDW). R_P is taken at 325 K for (a) and 400 K for (b) and (c).

IV. DISCUSSION

The two fundamental distinguishing properties in these films are stress and disorder. Grain sizes are similar in all but the bulklike sample, and yet three distinct reflectivity profiles are observed, so grain size alone is not a determining factor. However, the quality of the grain boundaries and surface roughness vary significantly, and defects within the grains are sources of disorder. We propose a low-temperature phase diagram for chromium as determined from our experimental

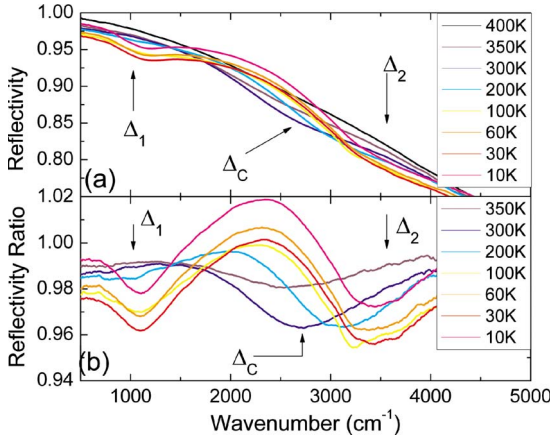

FIG. 6. (Color online) (a) Temperature dependent reflectivity and (b) reflectivity ratio ($R_L/R_{400\ \mathrm{K}}$) of the e-beam sample.

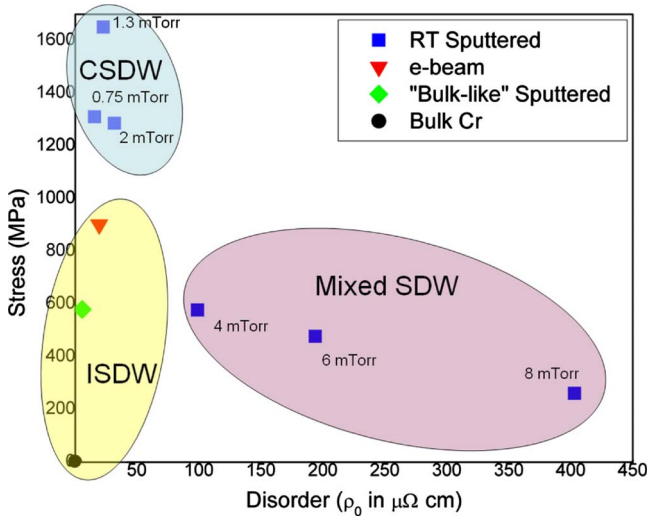

FIG. 7. (Color online) Phase diagram for the low-temperature magnetic state of Cr films in the disorder-stress plane. The axes are the residual resistivity ($\mu\Omega$ cm), representing disorder, and tensile stress (MPa). Phases are ISDW, CSDW, and mixed phase. The e-beam sample has a transition from ISDW to CSDW at 200 K, which is not accounted for in this low-temperature phase diagram.

results, with stress and disorder along the two axes, and show this in Fig. 7. For the y axis (stress) we have used the measured stress in the films (MPa), and on the x axis (disorder) we have used the residual resistivity ρ_0 ($\mu\Omega$ cm) listed for each sample in Table I. Each sample corresponds to a point on this map, with bulk Cr at the origin. Based on our reflectivity results, we demarcate three regions corresponding to the three SDW behaviors we observe: ISDW occurs in the region with low stress and low disorder, CSDW occurs in the region with high stress and low disorder, and mixed SDW phases occur in the region of low stress and high disorder. None of our samples fall into the region of high stress and high disorder.

This low-temperature phase diagram is almost entirely sufficient to describe the SDW behavior of our samples because all but one transition directly from their low-temperature behavior to the paramagnetic state, albeit at different Néel temperatures. Only the e-beam sample has an exclusively high-temperature SDW phase, exhibiting a transition ISDW→CSDW at around 200 K before transitioning to the paramagnetic state at around 400 K.

Let us focus on the stress dependence of the SDW by examining the samples with low disorder. The film with the lowest stress (bulklike) displays an ISDW behavior over the whole temperature range, while the films with the most stress (grown at 0.75, 1.3, and 2 mTorr) display a CSDW behavior over the whole temperature range. The film with stress between these, the e-beam sample, displays ISDW at low temperature and CSDW at higher temperatures. This dependence of SDW behavior on stress mirrors the dependence on Mn concentration described in the Introduction. In fact, it is surprising that so many of our samples showed CSDW *without* a lower temperature ISDW phase; this speaks to the very high stress present in the films.

While the ISDW→CSDW transition observed in the e-beam sample is not unusual,[1] it is particularly pertinent in this case because it corroborates the results of other studies done on e-beam deposited Cr.[2] Rotenberg *et al.* grew epitaxial Cr(110)/W(110) by e-beam evaporation and used *in situ* ARPES measurements to study very thin samples (30–120 Å). They observed a transition from ISDW →CSDW at a temperature that increased with increasing thickness. An extrapolation of their curve predicted that at large thicknesses, their films would still exhibit an ISDW →CSDW transition at 187 K, in disagreement with bulk behavior. Our 1500 Å film, grown under the same conditions (although not epitaxial or annealed), does, in fact, show such a transition near 200 K. This result supports the findings of Rotenberg *et al.*, and suggests that film stress plays a crucial role in this transition.

Next, let us focus on the mixed SDW samples. Unlike the e-beam sample, which shows different SDW behaviors in different temperature ranges, the mixed SDW samples exhibit multiple different SDW behaviors coexisting within the same temperature range. Previous work on crushed powders showed ISDW and CSDW coexisting within one sample; the coexistence disappeared upon annealing.[5] This suggests that coexisting phases are due to an inhomogeneous sample or defects in a sample. This is likely the case for our samples based on the inhomogeneity observed in the TEM images.

The most surprising result of the mixed SDW samples is that we observe an additional CSDW gap at 2400 cm^{-1}, like that observed in Cr-Al, coexisting with the ISDW and CSDW gaps, which we recognize from our other samples. Because we only observe the 2400 cm^{-1} gap in the high resistivity samples, we attribute it to regions with high defect concentrations, which are not present in the other films. In particular, we expect that materials at or near the grain boundaries contribute to this phase. The high resistivity found in Cr-Al alloys, as well as the theory that substitutional Al atoms act as vacancies in Cr,[1,12] gives support to the analogy that we draw between Cr-Al alloys and the most disordered regions of our high resistivity samples. As for the other gaps, the 3200 cm^{-1} CSDW gap, also observed in the 0.75, 1.3, and 2 mTorr films, and the ISDW gaps, also seen in the bulklike and e-beam samples, are attributed to regions of high crystalline quality, far from the grain boundaries. Either different amounts of tensile stress or different grain sizes observed throughout the thickness of the film cause the regions to differentiate between CSDW and ISDW.

V. CONCLUSIONS

In summary, we have used infrared spectroscopy to determine the spin-density wave properties of polycrystalline chromium thin films. The behavior of this system is strongly dependent on the deposition conditions, and the diversity of behavior is remarkable, considering that it includes only one element and a single bcc structure. Here, we highlight the main findings of this paper:

(1) We observe three types of SDW behavior at low temperature for polycrystalline Cr thin film samples:

(a) incommensurate SDW, in films with low stress and low disorder;

(b) commensurate SDW, in films with high stress and low disorder;

(c) mixed SDW, in films with low stress, high disorder, and an inhomogeneous microstructure.

(2) The film with the largest grains, lowest residual resistivity, and low stress (the bulklike sample, sputtered at 0.75 mTorr with the substrate at 350 °C) has a magnetic structure, which closely mimics bulk chromium.

(3) The e-beam sample showed an ISDW behavior at low temperature, transitioned to CSDW near 200 K, and became paramagnetic near 400 K. No other sample showed an ISDW→CSDW transition.

(4) Samples with mixed SDW had gaps corresponding to the ISDW and CSDW phases observed in the other samples, plus an additional gap at 2400 cm^{-1}, which we attribute to CSDW in highly disordered regions of the sample. We compare this gap to the one seen in CSDW Cr-Al alloys.

ACKNOWLEDGMENTS

The authors thank Michael C. Martin and Zhao Hao from the Advanced Light Source for assistance with infrared measurements, Eli Rotenberg from Lawrence Berkeley National Laboratory, Oleg Krupin from the Department of Physics, University of Oregon for assistance in the growth of the e-beam sample, and David J. Smith from Arizona State University for the TEM. This work was supported by the Director, Office of Science, Office of Basic Energy Sciences, Materials Sciences and Engineering Division, of the U.S. Department of Energy under Contract No. DE-AC02-05CH11231.

*zboekelheide@berkeley.edu

[1] E. Fawcett, H. L. Alberts, V. Yu. Galkin, D. R. Noakes, and J. V. Yakhmi, Rev. Mod. Phys. **66**, 25 (1994).

[2] E. Rotenberg, B. K. Freelon, H. Koh, A. Bostwick, K. Rossnagel, A. Schmid, and S. D. Kevan, New J. Phys. **7**, 114 (2005).

[3] J. S. Parker, L. Wang, K. A. Steiner, P. A. Crowell, and C. Leighton, Phys. Rev. Lett. **97**, 227206 (2006).

[4] M. C. Cyrille, S. Kim, M. E. Gomez, J. Santamaria, C. Leighton, K. M. Krishnan, and I. K. Schuller, Phys. Rev. B **62**, 15079 (2000).

[5] G. E. Bacon and N. Cowlam, J. Phys. C **2**, 238 (1969).

[6] I. S. Williams and R. Street, Philos. Mag. B **43**, 893 (1981).

[7] L. M. Falicov and David R. Penn, Phys. Rev. **158**, 476 (1967).

[8] Setsuro Asano and Jiro Yamashita, J. Phys. Soc. Jpn. **23**, 714 (1967).

[9] Laurence W. Bos and David W. Lynch, Phys. Rev. B **2**, 4567 (1970).

[10] A. Kallel and F. de Bergevin, Solid State Commun. **5**, 955

(1967).
[11] M. A. Lind and J. L. Stanford, J. Phys. Soc. Jpn. **53**, 4029 (1984).
[12] H. Akai and J. Kanamori, J. Phys. Soc. Jpn. **54**, 3537 (1985).
[13] The calculations for grain size corrected for instrumental broadening, which was small.
[14] An additional film was grown on a Si thermal oxide substrate, so at. % N could be measured without observing a signal from the SiN_x substrate. For at. % C, the EDS chamber had a background of 5 ± 1 at. % C signal, which obscured the measurement; the margin of error for the at. % C measurement is therefore 1 at. %.
[15] The stress in the e-beam sample was determined using x-ray diffraction by correlating the measured out-of-plane lattice constant to those of the other samples with known stress. This assumes a similar stress-strain relationship and Poisson's ratio for all the polycrystalline samples.
[16] D. W. Hoffman and John A. Thornton, J. Vac. Sci. Technol. **20**, 355 (1982).
[17] The source-substrate distance for our samples was about 20 cm.
[18] L. S. Suominen, C. Zhou, M. A. Korhonen, and C.-Y. Li, Adv. X-Ray Anal. **40**, 544 (1996).
[19] John A. Thornton and David W. Hoffman, J. Vac. Sci. Technol. **14**, 164 (1977).
[20] All films show a resistivity minimum below 100 K, and we report the residual resistivity as the resistivity at the minimum. The magnitude of the low-temperature upturn is small, representing no more than 1% of the total resistivity.
[21] E. E. Fullerton, K. T. Riggs, C. H. Sowers, S. D. Bader, and A. Berger, Phys. Rev. Lett. **75**, 330 (1995).
[22] M. A. Lind and J. L. Stanford, Phys. Lett. **39A**, 5 (1972).